Composites Part B 264 (2023) 110882

Contents lists available at ScienceDirect

Composites Part B

journal homepage: www.elsevier.com/locate/compositesb

A finite element model for the prediction of porosity in autoclave cured composites

Andrea Dei Sommi [a], Giuseppe Buccoliero [a,b], Francesca Lionetto [a], Fabio De Pascalis [c], Michele Nacucchi [c], Alfonso Maffezzoli [a,*]

[a] Department of Engineering for Innovation, University of Salento, via Monteroni, 73100, Lecce, Italy
[b] Advanced Materials and Processes Consulting Department, CETMA, Brindisi, Italy
[c] ENEA, Division for Sustainable Materials, Research Centre of Brindisi, S.S.7 Appia km 709, 72100, Brindisi, Italy

ARTICLE INFO

Handling Editor: Prof. Ole Thomsen

Keywords:
Thermosetting resin
Porosity
Finite element analysis (FEA)
Autoclave

ABSTRACT

Porosity represents a critical issue in composite manufacturing often leading to parts rejection. The aim of this work was to develop a multiphysic model capable to predict the conditions leading to porosity generated by water in composite parts processed by autoclave lamination. The developed model does not aim to assess the void growth phenomenon, as other models in the literature, but it enables the prediction of the thermodynamic conditions for water-generated porosity, where they could occur and how to prevent their presence by suitably modifying the process parameters. The potential of this multiphysic model was proved on epoxy matrix carbon fiber reinforced laminates cured after their exposition to a moist environment. The model was also applied to modify the curing cycle suggested by the prepreg provider in order to avoid favorable conditions for porosity development.

1. Introduction

Autoclave lamination is one of the most used techniques for the fabrication of composite parts in several fields, such as aerospace and aeronautics, mainly when high-performance and tight geometrical tolerances are needed, although out-of-autoclave (OoA) processes [1,2] and materials [3] have been introduced in order to reduce the costs and time required by the traditional autoclave methods [4]. In an autoclave lamination process, prepregs are laid-up to form a laminate, vacuum bagged with many auxiliary layers, and then cured in the autoclave. The gas (nitrogen) pressure in autoclave, which is typically in the order of 0.8 MPa for laminates and 0.4 MPa for sandwich panels, is applied to achieve laminate consolidation and defects suppression [5]. Porosity (or voids) represents one of the principal sources of defects leading to properties reduction and, in some cases, to parts rejection [6–13]. Voids are generated due to the presence of volatiles, especially air entrapped during the lay-up and absorbed moisture [14–16], which are responsible for void nucleation and growth [17]. In fact, considering that the prepreg thickness is typically less than 0.2 mm in aircraft parts, water absorption in prepregs is likely to occur during storage and in a clean room during lamination, up to the equilibrium with the environment is reached [18]. During the curing cycle, the increase in temperature allows the resin to react, promotes water desorption, and increases the vapor pressure of water. If the time for void nucleation is adequately shorter than the time needed for resin gelation and if the void pressure, which is equal to the water vapor pressure, is higher than the hydrostatic resin pressure, the void will potentially grow until the resin is in the liquid state [5]. After resin gelation, in fact, viscosity is too high and resin flow is stopped. The same phenomenology occurs if, aside from water, other volatile organic compounds are dissolved in the matrix. The resin flow through the composite thickness is responsible for pressure transfer from autoclave gas to liquid resin. Because of the difficulties in controlling all these phenomena related to void formation, the process parameters are generally set according to trial-and-error procedures.

A numerical model, integrating all complex phenomena involved in autoclave lamination, represents a useful tool to predict and prevent void formation during composite manufacturing. Most of the available numerical models for the prediction of void development [14,17,19] consider the void as a spherical gas bubble surrounded by a saturated liquid, an assumption far from the real complex shape of voids [20]. De Parscau du Plessix et al. [20] improved the classical model for the prediction of the spherical void growth including a boundary layer around

* Corresponding author.
E-mail address: alfonso.maffezzoli@unisalento.it (A. Maffezzoli).

https://doi.org/10.1016/j.compositesb.2023.110882
Received 23 February 2023; Received in revised form 21 June 2023; Accepted 30 June 2023
Available online 3 July 2023

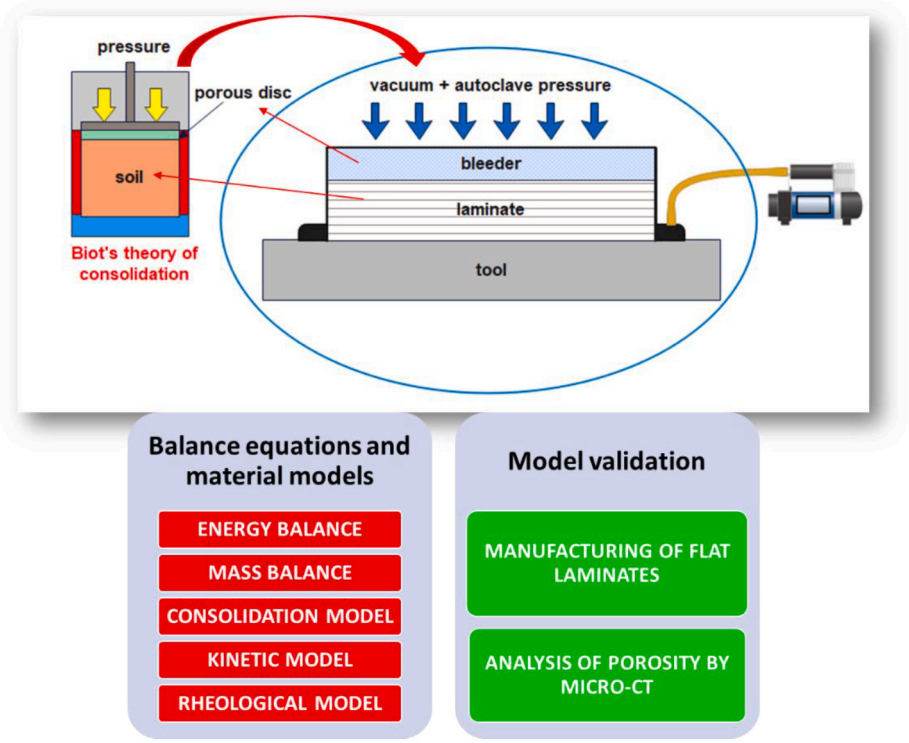

Fig. 1. Schematic of the multiphysic model for porosity prediction.

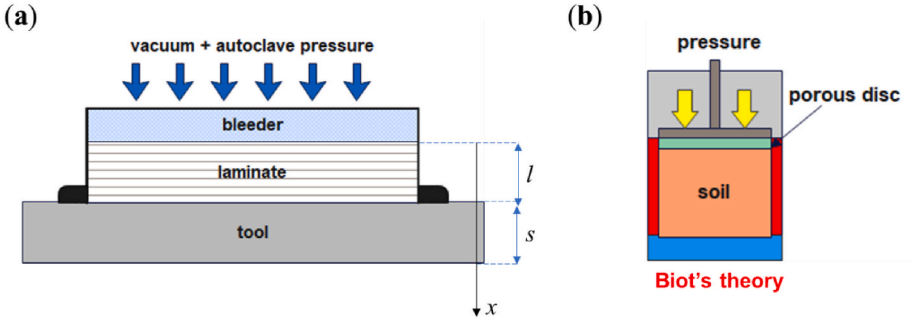

Fig. 2. (**a**) Sketch of the model domain (*l* and *s* are the laminate and tool thickness, respectively) and (**b**) sketch of Biot's theory.

the bubble with different diffusive properties in order to explain the lower water diffusion at the interface. Kermani et al. [21], instead, elaborated a physics-based model to calculate the porosity of the bond line during the co-cure of honeycomb core sandwich structures in an autoclave. They applied the void growth stability map of Kardos et al. [17] to design cure cycles allowing to avoid diffusion-induced void growth.

In a different way from these models, the aim of this work was not to predict the void growth but to develop a model able to determine if the conditions for void development, i.e., the presence of residual absorbed moisture and the comparison between water vapor pressure and hydrostatic resin pressure, are satisfied, and to properly choose the process parameters in order to prevent it. A multiphysic finite element model for the prediction of the potential porosity evolution in composite materials during the autoclave process was developed. As illustrated in Fig. 1, the proposed multiphysic approach includes energy, mass and force (i.e., a consolidation model) balance equations along with kinetic and rheological models, and was validated through the manufacturing of composite laminates and the analysis of their porosity after curing.

2. Model description

The developed model consists of five governing equations based on: (i) an energy balance for temperature calculation, accounting for the heat transfer across the composite laminate and the tool and the exothermal effect of the resin chemical reaction during curing, (ii) a mass balance, to calculate the moisture concentration through the composite thickness during the autoclave curing cycle, (iii) a consolidation model based on a force balance, exploiting the general theory of three-dimensional soil consolidation, to calculate the time-dependent resin hydrostatic pressure across the laminate thickness, (iv) a kinetic model, to calculate the evolution of the degree of reaction as a function of time and temperature, and (v) a rheological model, to calculate the evolution of the resin viscosity as a function of temperature and degree of reaction. As shown in Fig. 2a, a unidimensional model was developed adopting a domain given by a composite laminate of thickness *l* and a metal tool of thickness *s*.

2.1. Kinetic model

The kinetic model used for the cure of resin is a modified version of

Kamal's model [22] (Karkanas and Partridge's model [23]):

$$\frac{d\alpha}{dt} = k_1(1-\alpha)^{n_1} + k_2\alpha^m(1-\alpha)^{n_2} \tag{2.1}$$

where α (−) is the degree of reaction of resin, m (−), n_1 (−) and n_2 (−) are reaction orders, and k_1 (s^{-1}) and k_2 (s^{-1}) are kinetic constants with an Arrhenius dependence on temperature T (K):

$$k_i = k_{0i}e^{-\frac{E_{ai}}{RT}}, i = 1,2 \tag{2.2}$$

where k_{0i} (s^{-1}) is a pre-exponential factor, E_{ai} (J/mol) the apparent activation energy, and R (J/(mol*K)) the universal gas constant. In order to consider the effects of resin vitrification on cure, the term α_{max} (−) was introduced [24,25], which also depends on temperature and ranges between 0 and 1:

$$\frac{d\alpha}{dt} = k_1(\alpha_{max}-\alpha)^{n_1} + k_2\alpha^m(\alpha_{max}-\alpha)^{n_2} \tag{2.3}$$

$$\alpha_{max} = p + qT \tag{2.4}$$

where p (−) and q (K^{-1}) are two fitting parameters.

Although it is reported that water absorption can determine a change in curing kinetics [26], this effect was neglected considering that the uncured resin in clean room conditions absorbs less than 1%. Moreover, water desorption during heating before the onset of polymerization further decreases the water content in the resin.

2.2. Rheological model

The rheological model is based on Lionetto et al. [27] modified version of Kenny and Opalicki model [28] considering the twofold effect of temperature, since on the one hand an increase of temperature lowers the resin viscosity but on the other hand induces the resin reaction thus increasing its viscosity η (Pa*s):

$$\eta = \eta_{g0}e^{\left[\frac{C_1(T-T_{g0})}{C_2+T-T_{g0}}\right]\left[\frac{\alpha_g}{\alpha_g-\alpha}\right]^{A+B\alpha}} \tag{2.5}$$

where η_{g0} (Pa*s) is the viscosity of the unreacted resin at the initial glass transition temperature T_{g0} (K), α_g (−) the degree of reaction at gel temperature, and A (−), B (−), C_1 (−) and C_2 (K) are model parameters.

2.3. Consolidation model

The reinforcement is characterized by a non-linear stress-strain relation. The load taken by the reinforcement stack σ (Pa) can be fitted with an exponential growth function [29]:

$$\sigma = A_0\left(e^{\varepsilon/A_1} - 1\right) \tag{2.6}$$

where A_0 (Pa) and A_1 (−) are model parameters and ε (−) is the deformation given by the resin flow across the bleeder. In order to overcome some limitations of the model formerly proposed [29] which assumed a constant hydrostatic resin pressure across the laminate thickness according to Kelvin-Voigt-like behavior, Biot's theory was implemented by Buccoliero et al. [30] to take into account the variation of resin pressure through the laminate thickness. Biot's theory was appropriately adapted to the case of resin flow during the consolidation of a laminate assuming the prepreg stack as a column of soil fully impregnated of water supporting an external pressure and laterally confined in a rigid sheath, as sketched in Fig. 2b. As the thickness of the reinforcement is reduced as a consequence of the pressure applied through bag and bleeder, resin flows through it filling the bleeder until it makes contact with the bag.

$$\frac{\partial}{\partial x}\left(\lambda\frac{\partial P}{\partial x}\right) = \frac{\partial P}{\partial t} \tag{2.7}$$

$$\lambda = \frac{K}{\eta \bullet a} \tag{2.8}$$

$$a = \frac{1-2\nu}{2G(1-\nu)} \tag{2.9}$$

where P (Pa) is the resin pressure, t (s) the time, λ (m^2/s) the consolidation constant, K (m^2) the transversal Darcy's permeability of the reinforcement [31,32], a (Pa^{-1}) the final reinforcement compressibility, and G (Pa) and ν (−) are the reinforcement shear modulus and Poisson's modulus, respectively.

2.4. Mass balance

Fick's second law of diffusion [33] was used to calculate the moisture concentration c (mol/m^3), which is the absolute amount of absorbed moisture expressed as the mass of moisture per unit volume:

$$\frac{\partial c}{\partial t} = D\frac{\partial^2 c}{\partial x^2} \tag{2.10}$$

where x (m) is the through-the-thickness direction and D (m^2/s) the diffusivity, assumed not dependent on the space variable x. In materials characterized by an ideal Fickian behavior, such as the liquid resin used in prepregs [34], this property is assumed independent of the moisture exposure level and thus of the moisture equilibrium content. However, the moisture diffusivity coefficient is strongly influenced by temperature and, in the case of diffusion of water in the uncured or cured prepreg, it follows an Arrhenius-type equation [35]:

$$D = D_0e^{-\frac{E_{ad}}{RT}} \tag{2.11}$$

where D_0 (m^2/s) is the pre-exponential constant, E_{ad} (J/mol) the activation energy for diffusion per mole, R (J/(mol*K)) the universal gas constant, and T (K) the absolute temperature. In the case of an autoclave process, after application of the vacuum bag, either at room temperature either during the heating step, the moisture previously absorbed by resin will be desorbed. The diffusion coefficient of the composite laminate was obtained from that of the resin according to the Bharadwaj's model [36], which describes the diffusive permeability in filled polymers. When Henry's and Darcy's laws hold, as in liquid epoxy resins, permeability is given by the product of solubility and diffusion coefficient. Considering that solubility in the composite can be attributed only to the resin and that it is an equilibrium property not dependent on the type and geometry of the filler, it is possible to estimate the diffusion coefficient through the thickness (out-of-plane) of a composite laminate from the value determined for resin:

$$D_c = D_r\left(1-V_f\right) \tag{2.12}$$

where D_c (m^2/s) and D_r (m^2/s) are the composite and resin diffusion coefficient, respectively, and V_f (−) is the fiber volume fraction. Being the aspect ratio of reinforcement in out-of-plane direction equal to 1, only V_f is responsible of the difference between D_c and D_r.

2.5. Energy balance

An energy balance was introduced in order to consider the heat transfer across the composite laminate and the tool and the exothermal effect of the chemical reaction of the resin during the curing process. For the energy balance two assumptions were considered, a flat plane geometry, as usually occurs in composite laminates, and constant properties of the composite. The resulting equation is [37,38]:

Table 1
Initial and boundary conditions (l and s are laminate and tool thickness, respectively).

Initial conditions	$P(x,t) = P_{aut}, 0 \le x \le l$ (2.14) $c(x,t) = c_0, 0 \le x \le l$ (2.15) $T(x,t) = T_0, 0 \le x \le l+s$ (2.16)
Boundary conditions	$P(x,t) = 0, x = 0$ (2.17) $c(x,t) = 0, x = 0$ (2.18) $\frac{\partial P(x,t)}{\partial x} = 0, x = l$ (2.19) $\frac{\partial c(x,t)}{\partial x} = 0, x = l$ (2.20) $-k_c\frac{\partial T}{\partial x} = h_c(T - T_e), x = 0$ (2.21) $-k_t\frac{\partial T}{\partial x} = h_c(T - T_e), x = l+s$ (2.22)

$$\rho_c c_{pc}\frac{\partial T}{\partial t} = k_c\frac{\partial^2 T}{\partial x^2} + \rho_c \Delta h_{ref}\frac{d\alpha}{dt} \quad (2.13)$$

where ρ_c (kg/m^3) is the composite density, c_{pc} (J/(kg*K)) the composite specific heat, k_c (W/m*K) the composite thermal conductivity in the through-the-thickness direction x (m), and Δh_{ref} (J/kg) the heat generated by the chemical reaction.

The initial and boundary conditions of the model are listed in Table 1. The first initial condition (Equation 2.14) results from the high stiffness of the stack considering that the uncured resin behaves as a solid at room temperature, being P_{aut}, the autoclave pressure, usually set to 0.8 MPa. The second and third initial conditions (Equations 2.15 and 2.16) refer to the initial value of moisture concentration c_0 and temperature T_0, respectively. T_0 is assumed equal to room temperature and c_0 equal to the equilibrium water content achieved in clean room conditions where 50% Relative Humidity (RH) is imposed. The first two boundary conditions (Equations 2.17 and 2.18) refer to the laminate region which is in contact with the bleeder (dry environment under vacuum bag conditions, i.e., pressure of a few millibars), while the third and fourth conditions (Equations 2.19 and 2.20) refer to the laminate region which is in contact with the impermeable side of the tool. The last two boundary conditions (Equations 2.21 and 2.22) are convective boundary conditions since forced air convection is the major source of heat transfer in the autoclave, where h_c is the heat transfer coefficient (assumed equal to 40 W/(m^2*K) [38,39]), T_e the gas temperature in the autoclave, and k_c and k_t are the thermal conductivity of the composite and the tool, respectively.

3. Experimental

The input parameters of each model are summarized in Table 2, where the required experimental tests are also pointed out.

3.1. Materials

CYCOM® 977–2 toughened epoxy resin and CYCOM® 977-2-34%-24KIMS-196 carbon/epoxy unidirectional tape with a weight of 196 g/m^2 (Solvay) were investigated in this work. The bleeder material was the Airweave® N10 (Airtech) heavy weight non-woven polyester breather.

Table 2
Input parameters and experimental tests required for the five models.

Models	Input parameters	Experimental tests
Kinetic model	k_{01}, E_{a1}, n_1, k_{02}, E_{a2}, n_2, m, p, q	Differential scanning calorimetry analysis on uncured resin
Rheological model	η_{g0}, T_{g0}, α_g, A, B, C_1, C_2	Rheological analysis on uncured resin
Consolidation model	A_0, A_1, K	Compression and permeability tests on dry reinforcement
Mass balance	D_0, E_{ad}	Absorption and desorption tests on uncured resin
Energy balance	Δh_{ref}	Differential scanning calorimetry analysis on uncured resin

3.2. Methods

The experimental input parameters are listed in Table 3. The parameters for the kinetic and rheological models and the energy balance were taken or extrapolated from Lionetto et al.'s [29] work. The parameters for the consolidation model were obtained from the fitting of the compression tests performed on the dry reinforcement of the prepreg used for the production of laminates, as reported in Supplementary materials. Water absorption and desorption tests were performed on epoxy resin samples. The material properties, instead, were taken from online databases [40].

3.2.1. Absorption and desorption tests

Absorption and desorption tests were performed on resin disks with a diameter of 50 mm and a thickness of 1 mm using a Binder KMF 115 climate chamber under different temperature and relative humidity levels. Each sample was dried under vacuum before the exposition to the moist environment. The tests were carried out at five different temperatures (30, 40, 60, 70, and 75 °C) and two humidity levels (50% and 75 %RH). The minimum temperature of 30 °C was chosen to allow a proper control of the experimental conditions. The maximum temperature of 75 °C allowed to avoid resin gelation during desorption experiments. Weight change measurements showed a Fickian behavior according to the ASTM D5229/D5229M − 20 standard [42]. The parameters D_0 and E_{ad} of Equation (2.11) were obtained by fitting D values and then D_c was calculated from Equation (2.12).

3.2.2. Sample curing and void content evaluation

Model validation was achieved by evaluating the final porosity of composite samples, which were conditioned at a temperature of 30 °C and two RH levels, 50% and 75 %RH, until saturation and cured at three pressure levels (0.1, 0.4, and 0.8 MPa) heating at 2 °C/min up to the curing temperature of 180 °C and kept in isothermal conditions for 3 h, according to the suggested curing cycle of prepreg manufacturer. Each laminate with a fiber content of 59 ± 2% by volume had a $[0_{30}]_T$ stacking sequence and a bleeder with a thickness of 0.15 mm was used during the curing process. The porosity was measured by density measurements according to the ASTM D792-20 standard [43] on at least five samples with 40 × 10 mm^2 dimensions cut from the composite laminates.

The distribution and morphology of voids in the cured laminates were examined by micro-CT (samples of about 5 × 5 × 2 mm^3) [44]. The tomographic analyses were performed in the laboratory of the ENEA research center of Brindisi (Italy). A GE Phoenix Nanotom CT system equipped with a 180 kV/15 W nano-focus X-ray tube was used. The scan resolution (voxel size) was set to 15 μm. On the one hand, this resolution

Table 3
Experimental input parameters of the model.

A_0	A_1	m[29]	n_1 [29]	n_2 [29]	k_{01} [29]
(Pa)	(-)	(-)	(-)	(-)	(s^{-1})
1.11*10^4	6.50*10^{-2}	5.80*10^{-1}	7.90*10^{-1}	1.99	1.15*10^{10}
k_{02} [29]	E_{a1} [29]	E_{a2} [29]	η_{g0} [29]	T_{g0} [29]	α_g [29]
(s^{-1})	(J/mol)	(J/mol)	(Pa s)	(K)	(-)
1.40*10^2	1.27*10^5	4.51*10^4	6.05*10^{10}	2.66*10^2	4.55*10^{-1}
A [29]	B [29]	C_1 [29]	C_2 [29]	Δh_{ref} [29]	P [29]
(-)	(-)	(-)	(K)	(J/kg)	(-)
5.98	8.05	3.45*10^1	5.31*10^1	3.56*10^5	-2.54
Q [29]	K [41]	ρ_c [40]	c_{pc} [40]	k_c [40]	ρ_t [40]
(K^{-1})	(μm^2)	(kg/m^3)	(J/kgK)	(W/mK)	(kg/m^3)
7.40*10^{-3}	5.10*10^{-2}	1.59*10^3	8.71*10^2	4.03*10^{-1}	2.70*10^3
c_{pt} [40]	k_t [40]	D_0	E_{ad}	l	s
(J/kgK)	(W/mK)	(m^2/s)	(J/mol)	(m)	(m)
9.00*10^2	1.45*10^2	1.90*10^{-2}	5.55*10^4	5.58*10^{-3}	2.00*10^{-2}

Table 4
Case studies and predicted resin and reinforcement pressures at the end of the flow.

Laminate		Autoclave pressure (MPa)
50 %RH	75 %RH	
1L	2L	0.1
3L	4L	0.4
5L	6L	0.8

allows even the smallest pores to be highlighted, but on the other hand it allows only a part of the samples to be imaged. Therefore, the porosity analysis was limited to the central area of the samples only, whose planar dimensions were 2.7 × 2.7 mm^2.

4. Model results and validation

This multiphysic finite element model, integrating the coupled differential equations given by mass, energy and force balances with kinetic and rheological models, is able to predict the distribution of resin pressure, water concentration, temperature, degree of reaction, and viscosity across composite laminates of different thicknesses during a curing cycle, also accounting for bleeder thickness affecting the resin flow and pressure transfer from autoclave gas to resin. The FlexPDE software (PDE Solutions Inc.) was used to simultaneously solve the governing equations of the model. The case studies are labeled as 1L and 2L for laminates cured at 0.1 MPa and conditioned at 50 %RH and 75 % RH, respectively, 3L and 4L for laminates cured at 0.4 MPa and conditioned at 50 %RH and 75 %RH, respectively, and 5L and 6L for laminates cured at 0.8 MPa and conditioned at 50 %RH and 75 %RH, respectively, as schematically reported in Table 4.

4.1. Model results

The simulations have been stopped at gel point because at gelation resin becomes rubbery and viscosity increases enough to stop the resin flow and to prevent any further void nucleation and growth. Fig. 3 shows the concentration of water as a function of time at the midplane and tool side of all laminates. The initial concentration of water, calculated from the amount of moisture absorbed by resin until saturation, is 281 mol/m^3 and 727 mol/m^3 for the laminates conditioned at 50 %RH and 75 %RH, respectively. Even if moisture absorption changes over the lay-up time and the laminate has not reached equilibrium when enters autoclave, saturation condition has been chosen since it represents the worst condition promoting void development. As a results of simulation, water desorption is not complete in all cases, so if water vapor pressure exceeds resin pressure before gelation, the conditions for porosity development are satisfied.

Fig. 4 shows the resin pressure at the tool side of the laminate, which is the more critical region regarding voids development due to the higher concentration of residual moisture, as shown by Fig. 3. The water vapor pressure P_{water} (Pa) evolution, calculated from Equation (4.1) as a function of temperature T (°C) (Arden Buck equation [45]), and viscosity evolution are also reported until resin gelation, which occurs at about 150 min.

$$P_{water} = 611.21e^{\left(18.678-\frac{T}{234.5}\right)\left(\frac{T}{257.14+T}\right)} \quad (4.1)$$

The water vapor pressure exceeds the resin pressure at about 53 min for specimens 1L and 2L, while the resin viscosity is decreasing; at about 76 min for specimens 3L and 4L, when the resin viscosity is close to the minimum value; at about 95 min for the specimens 5L and 6L, when the resin viscosity is at the minimum value.

In all these cases, water vapor pressure exceeds resin pressure when resin viscosity is still very low. Thus, void formation conditions are satisfied. The resin flow ends due to the complete filling of the bleeder and only a very small fraction of the autoclave pressure is taken by the elastic reaction of the reinforcement. So, the pressure of the autoclave is almost completely transferred to the resin across the laminate thickness.

4.2. Model validation

Flat laminates were manufactured according to the same conditions simulated in Section 4.1. Micro-CT analysis was adopted to evaluate the porosity distribution along the thickness and the porosity shape. The porosity distribution was then compared to the porosity trend obtained by the proposed model. Porosity is generated where residual moisture remains before resin gelation and the resin pressure does not exceed the water vapor pressure inside the void, as predicted by the model. Table 5 summarizes the void content measured by density measurements.

A 3D rendering of the defects map obtained by the micro-CT analysis

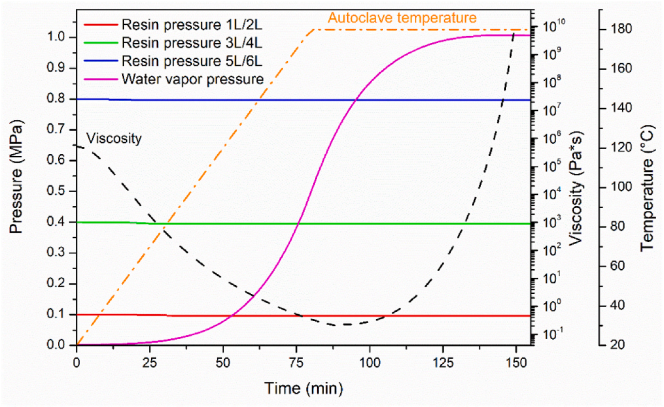

Fig. 4. Time dependence of gas temperature in autoclave, resin pressure and viscosity, and water vapor pressure at tool side of all laminates.

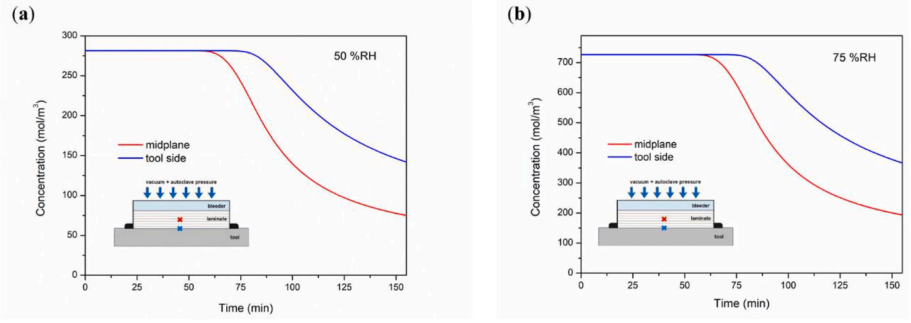

Fig. 3. Time dependence of moisture concentration at midplane (red cross) and tool side (blue cross) for all laminates conditioned at (**a**) 50 %RH and (**b**) 75 %RH. (For interpretation of the references to colour in this figure legend, the reader is referred to the Web version of this article.)

Table 5
Porosity values detected through micro-CT analysis.

Laminate	Autoclave pressure (MPa)	Humidity level (%RH)	Initial moisture concentration c_0 (mol/m^3)	Porosity (%)
1L	0.1	50	$2.81*10^2$	6.10
2L	0.1	75	$7.27*10^2$	7.38
3L	0.4	50	$2.81*10^2$	3.18
4L	0.4	75	$7.27*10^2$	4.26
5L	0.8	50	$2.81*10^2$	0.92
6L	0.8	75	$7.27*10^2$	1.51

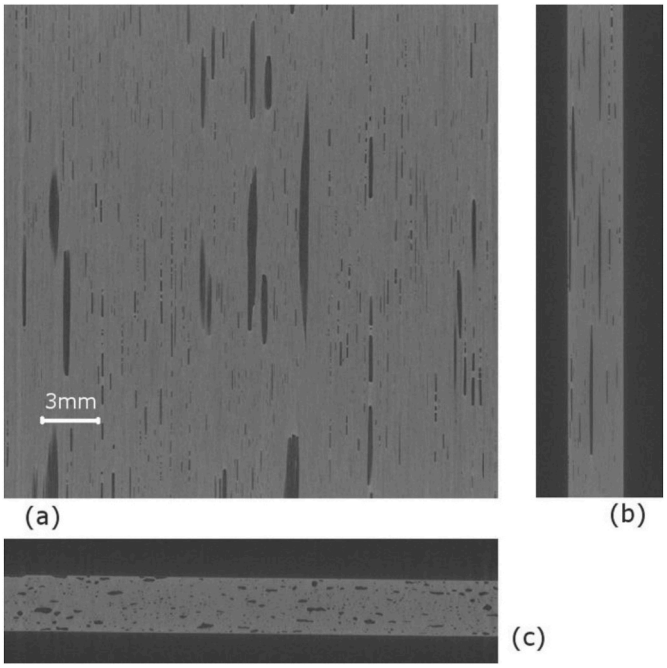

Fig. 5. Sample 1L: (**a**) transverse section, (**b**) longitudinal section, and (**c**) frontal section. Note that the tool side is at the bottom of picture **c**.

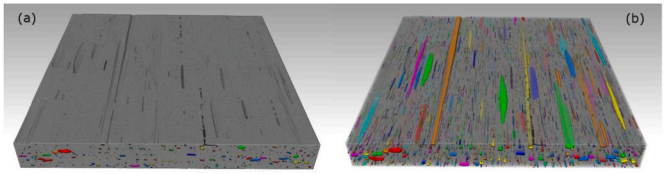

Fig. 6. Sample 1L: (**a**) 3D volume rendering and (**b**) transparent view of the porosity analysis in 3D. Tool side at bottom.

for samples 1L and 5L is reported in Figs. 5 and 6 and Figs. 7 and 8, respectively. Different sections (longitudinal, frontal, transverse) are shown. The porosity, detected through the micro-CT analysis, is characterized by a void shape that is not spherical but elliptical, with a main axis, much longer than the other, parallel to fibers. This result suggests that heterogeneous nucleation is promoted at the fiber surfaces and suggests that the theories available in the literature, which assume homogeneous nucleation and spherical voids, need to be improved. From Table 5 it is clear that the laminates conditioned at 75 %RH are characterized by higher porosity than the ones conditioned at 50 %RH and cured at the same pressure due to the higher residual moisture. All the laminates with the exception of those 1L and 2L show a prevalence of porosity at the tool side where, as shown in Fig. 3, the proposed model predicts a higher water content, and the water vapor pressure exceeds the resin pressure before the gelation, as reported in Fig. 4. As shown in

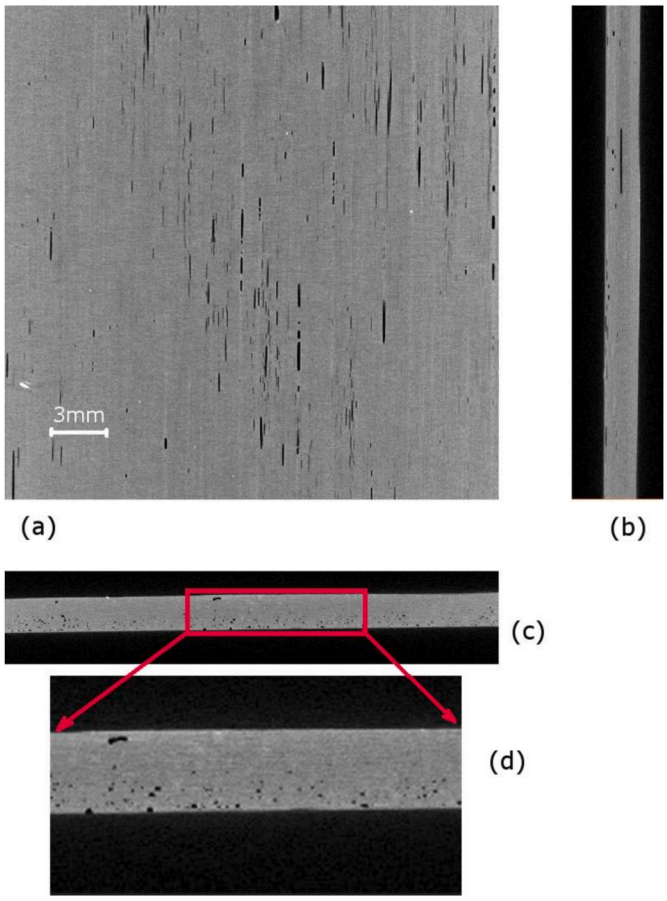

Fig. 7. Sample 5L: (**a**) transverse section, (**b**) longitudinal section, (**c**) frontal section, and (**d**) a close-up view showing pores placed in prevalence at the bottom of the sample (tool side).

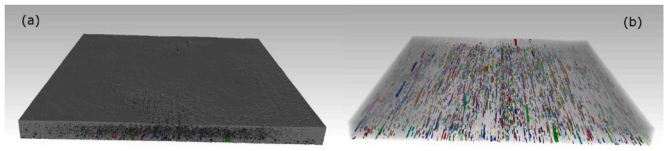

Fig. 8. Sample 5L: (**a**) 3D volume rendering and (**b**) transparent view of the porosity analysis in 3D. Tool side at bottom.

Fig. 5, the porosity is located along the entire thickness for the laminate 1L cured at 0.1 MPa. This occurs because the resin pressure is too low to counteract the water vapor pressure of the residual moisture content throughout the laminate thickness.

These results validated the developed model since the regions where the porosity was detected correspond to those where the model predicted a higher presence of residual moisture and a resin pressure lower than the water vapor pressure.

This model can be applied to simulate a variety of conditions, from water desorption at room temperature after vacuum bagging to the evaluation of the water desorption time in autoclave and low pressure OoA processes. The model can be also used to properly choose the bleeder thickness and temperature profiles, which affect respectively the resin pressure or the water vapor pressure before gelation, in order to limit the risk of porosity development.

As an example, to avoid water-induced porosity in a laminate conditioned at 50 %RH, the model was applied to include a dwell stage at intermediate temperatures in the curing cycle with the aim of promoting resin gelation by keeping resin hydrostatic pressure always

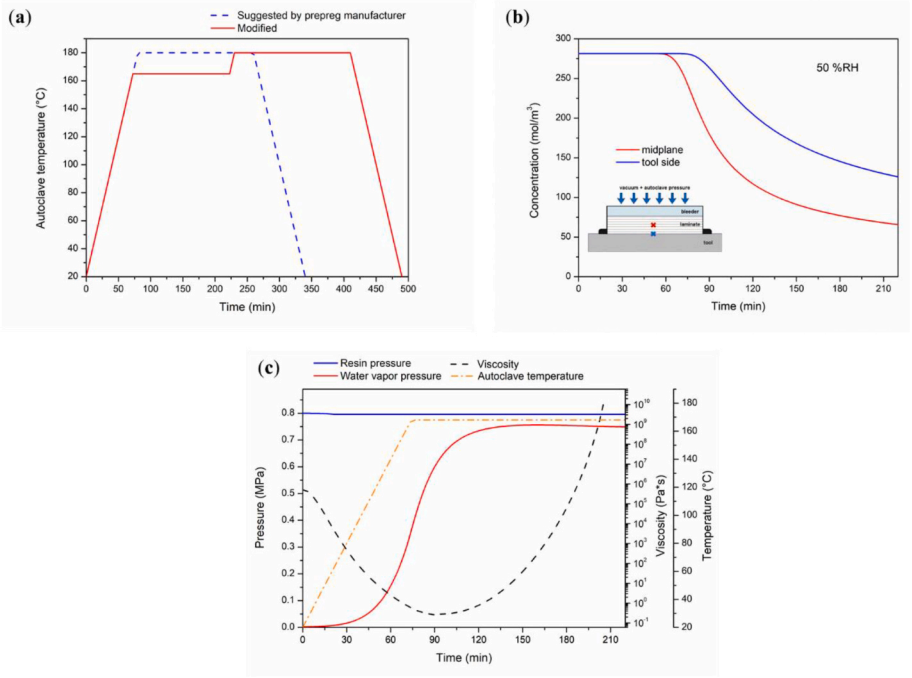

Fig. 9. Modified curing cycle: (**a**) comparison between the curing cycle suggested by the prepreg manufacturer and the modified curing cycle, (**b**) time dependence of moisture concentration at midplane (red cross) and tool side (blue cross) for a laminate conditioned at 50 %RH, and (**c**) time dependence of gas temperature in autoclave, resin pressure and viscosity, water vapor pressure at tool side. (For interpretation of the references to colour in this figure legend, the reader is referred to the Web version of this article.)

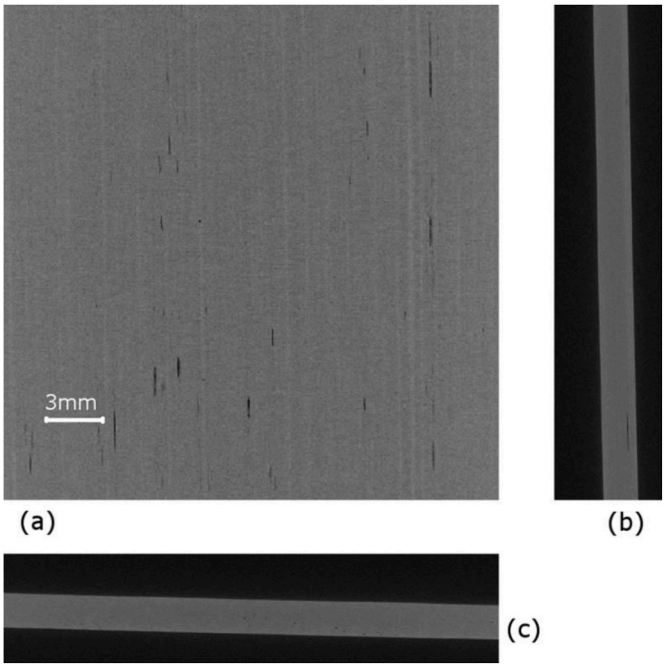

Fig. 10. Modified curing cycle: (**a**) transverse section, (**b**) longitudinal section, and (**c**) frontal section.

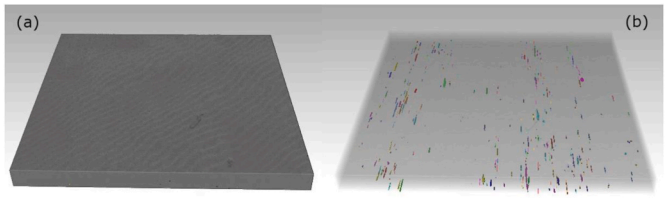

Fig. 11. Modified curing cycle: (**a**) 3D volume rendering and (**b**) transparent view of the porosity analysis in 3D. Tool side at bottom.

higher than water vapor pressure. The temperature and time of the dwell stage were properly tuned limiting as much as possible the increase of cycle time. The result was the inclusion of a dwell of 150 min at a temperature of 165 °C allowing curing at a reasonable rate while keeping water vapor pressure below hydrostatic pressure in the resin. After gelation, the curing cycle was then completed with a further step at 180 °C for 3 h, needed to reach both the target values of glass transition temperature and the degree of reaction for resin (Fig. 9a). Fig. 9b shows the concentration versus time curves at the midplane and tool side of the laminate cured with the modified thermal cycle. Also in this case, water desorption is not complete before gelation, which occurs at about 210 min, so it is necessary to compare the water vapor pressure with the resin pressure. Fig. 9c shows the resin viscosity and pressure at the tool side of the laminate. The selected dwell temperature allows reaching resin gelation while keeping the water vapor pressure lower than resin pressure over the entire dwell time counteracting any possible porosity growth caused by the residual moisture resin. These results were confirmed by the micro-CT analysis on the cured laminate (Figs. 10 and 11), which has a very low void content, equal to 0.045%.

A huge number of process variables values can affect the development of porosities and can be predicted by the proposed model such as:

- Laminate properties: composite, tool and bleeder thickness, reinforcement stiffness, reinforcement permeability, water diffusion coefficient, thermal properties of the composite and of the tool, curing kinetics, resin chemorheology;
- Initial and boundary conditions: initial water content in the resin, time at room temperature under vacuum, autoclave temperature and pressure profiles and convective heat transfer conditions.

In order to show the potential of the proposed model the case study of curing of the skin of a sandwich panel is presented. A thin skin, in the order of a few millimeters, is usually adopted and curing is performed at a gas pressure in an autoclave of 0.4 MPa, to prevent core crushing. Fig. 12a shows the concentration of water as a function of time and Fig. 12b the change in resin pressure and reinforcement stress for a laminate with a thickness of 1.5 mm cured at 0.4 MPa with two different

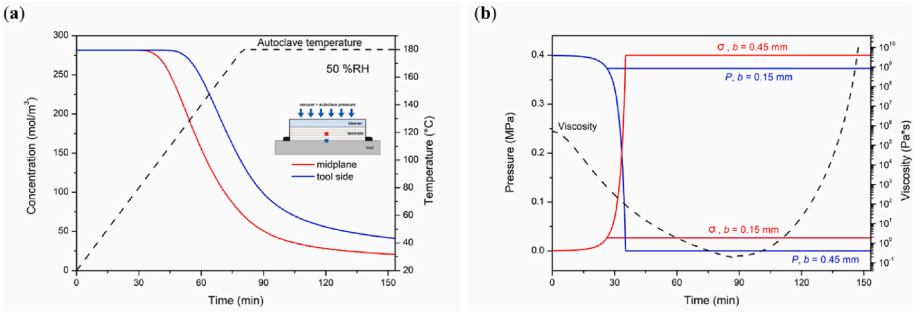

Fig. 12. (**a**) Time dependence of gas temperature in autoclave and moisture concentration at midplane (red cross) and tool side (blue cross) of the laminate and (**b**) time dependence of resin pressure (P) and viscosity and reinforcement stress (σ) at tool side (b is the bleeder thickness). (For interpretation of the references to colour in this figure legend, the reader is referred to the Web version of this article.)

values of the bleeder thickness, 0.15 mm and 0.45 mm. In the latter case, the bleeder thickness is too high (over-bleeding condition) and resin pressure goes to zero at about 35 min, when the water content is still high and viscosity is decreasing. These conditions will very likely promote the development of porosity.

5. Conclusions

A finite element model able to predict the potential conditions for porosity development in composite materials during the autoclave process was developed combining different balance equations coupled with models of material behavior. The model is based on the simultaneous solution of energy and mass balances coupled with kinetic, rheological, and consolidation models in order to predict the distribution of water concentration, temperature, resin pressure, and degree of reaction across composite laminates of different thicknesses during an autoclave curing cycle. In order to validate the developed multiphysic model, laminate samples, conditioned at different humidity levels and then cured at several autoclave pressure, were manufactured. The samples were analyzed by micro-CT to obtain the distribution and morphology of the voids developed during curing, while the void content was measured by density measurements. The micro-CT analysis detected porosity in the manufactured laminate, mainly at the tool side, where the model predicted higher residual moisture content. The elongated shape of voids indicated that fibers act as nucleation sites, suggesting that all former studies, which assumed spherical bubble growth, are not close to experimental evidence. The proposed model was used to modify the curing cycle suggested by the prepreg provider in order to keep the water vapor pressure lower than the hydrostatic resin pressure until resin gelation. These are the thermodynamic conditions to avoid porosity development while keeping the other conditions unchanged. A laminate conditioned at 50 %RH was manufactured according to this modified thermal cycle, which presented a very low void content (0.045%) thus confirming the model prediction.

The model can be used to predict the time evolution of each variable across the composite thickness during curing accounting for a huge number of variables that cannot be here addressed. For instance, changing the breather thicknesses, different resin pressure levels and related porosity content can be achieved for the same composite laminate, or a longer time spent under vacuum at room temperature can determine a lower moisture content in the laminate when viscosity is close to its minimum. This model can be also applied to the fabrication of composite parts used in any other application where different choices of auxiliary materials, clean room environmental conditions and temperature and pressure profiles are used. In some cases, lamination is performed in uncontrolled temperature and RH conditions. For the sake of brevity, only a case study and simulation of the adopted experimental set-up are reported in the paper but a huge number of different geometries, materials, lamination and curing conditions can be found when parts are fabricated for automotive, sport, general aviation, boat manufacturing industries.

In a future work, a heterogeneous nucleation model will be integrated to predict the void nucleation and growth phenomena.

Authorship statement

Conception and design of study: Maffezzoli, Lionetto, Buccoliero, Dei Sommi,

acquisition of data: Nacucchi, De Pascalis, Buccoliero, Lionetto; Dei Sommi

analysis and/or interpretation of data: Maffezzoli, Lionetto, Dei Sommi, Buccoliero.

Drafting the manuscript: Dei Sommi, Lionetto, Maffezzoli,

revising the manuscript critically for important intellectual content: Maffezzoli, Lionetto, Buccoliero, Dei Sommi.

Approval of the version of the manuscript to be published (the names of all authors must be listed): Dei Sommi, Buccoliero, Lionetto, De Pascalis, Nacucchi, Maffezzoli.

Declaration of competing interest

The authors declare that they have no known competing financial interests or personal relationships that could have appeared to influence the work reported in this paper.

Data availability

Data will be made available on request.

Acknowledgements

Mr. Francesco Montagna is kindly acknowledged for his support to experimental activities.

Appendix A. Supplementary data

Supplementary data to this article can be found online at https://doi.org/10.1016/j.compositesb.2023.110882.

References

[1] Louis B, Ermanni P. Out-of-Autoclave prepreg processing. Wiley Encyclopedia of Composites; 2012. https://doi.org/10.1002/9781118097298.WEOC056.

[2] Ekuase OA, Anjum N, Eze VO, Okoli OI. A review on the out-of-autoclave process for composite manufacturing. J. Compos. Sci. 2022;6:172. https://doi.org/10.3390/JCS6060172.

[3] Centea T, Grunenfelder LK, Nutt SR. A review of out-of-autoclave prepregs – material properties, process phenomena, and manufacturing considerations. Compos Part A Appl Sci Manuf 2015;70:132–54. https://doi.org/10.1016/J.COMPOSITESA.2014.09.029.

[4] van Hattum FWJ, Regel F, Labordus M. Cost reduction in manufacturing of aerospace composites. Plast, Rubber Compos 2011;40:93–9. https://doi.org/10.1179/174328911X12988622801052.

[5] Campbell FC, Mallow A, Browning C. Porosity in carbon fiber composites an overview of causes. J Adv Mater 1995;26:18–33.

[6] Muller de Almeida SF, Zabulon dos Santos N. N. Effect of void content on the strength of composite laminates. Compos Struct 1994;28:139–48. https://doi.org/10.1016/0263-8223(94)90044-2.

[7] Olivier P, Cottu JP, Ferret B. Effects of cure cycle pressure and voids on some mechanical properties of carbon/epoxy laminates. Composites 1995;26:509–15. https://doi.org/10.1016/0010-4361(95)96808-J.

[8] Costa ML, Almeida SFM de, Rezende MC. The influence of porosity on the interlaminar shear strength of carbon/epoxy and carbon/bismaleimide fabric laminates. Compos Sci Technol 2001;61:2101–8. https://doi.org/10.1016/S0266-3538(01)00157-9.

[9] Liu L, Zhang BM, Wang DF, Wu ZJ. Effects of cure cycles on void content and mechanical properties of composite laminates. Compos Struct 2006;73:303–9. https://doi.org/10.1016/J.COMPSTRUCT.2005.02.001.

[10] Chambers AR, Earl JS, Squires CA, Suhot MA. The effect of voids on the flexural fatigue performance of unidirectional carbon fibre composites developed for wind turbine applications. Int J Fatig 2006;28:1389–98. https://doi.org/10.1016/J.IJFATIGUE.2006.02.033.

[11] Mehdikhani M, Gorbatikh L, Verpoest I, Lomov S v. Voids in fiber-reinforced polymer composites: a review on their formation, characteristics, and effects on mechanical performance. J Compos Mater 2019;53:1579–669. https://doi.org/10.1177/0021998318772152/ASSET/IMAGES/LARGE/10.1177_0021998318772152-FIG2.JPEG.

[12] Baghad A, el Mabrouk K. Vacuum-pressure effects on microstructure and mechanical properties of autoclaved epoxy/carbon composite laminates. Iran Polym J (Engl Ed) 2022;31:1237–46. https://doi.org/10.1007/S13726-022-01072-6/TABLES/2.

[13] Fraga AN, Alvarez VA, Vázquez A, de La Osa O. Relationship between dynamic mechanical properties and water absorption of unsaturated polyester and vinyl ester glass fiber composites. J Compos Mater 2003;37:1553–74. https://doi.org/10.1177/0021998303029421.

[14] Wood JR, Bader MG. Void control for polymer-matrix composites (1): theoretical and experimental methods for determining the growth and collapse of gas bubbles. Compos Manuf 1994;5:139–47. https://doi.org/10.1016/0956-7143(94)90023-X.

[15] Grunenfelder LK, Nutt SR. Void formation in composite prepregs – effect of dissolved moisture. Compos Sci Technol 2010;16:2304–9. https://doi.org/10.1016/J.COMPSCITECH.2010.09.009.

[16] Anderson JP, Altan MC. Formation of voids in composite laminates: coupled effect of moisture content and processing pressure. Polym Compos 2015;36:376–84. https://doi.org/10.1002/PC.22952.

[17] Kardos JL, Duduković MP, Dave R. Void growth and resin transport during processing of thermosetting — matrix composites. In: Dušek K, editor. Epoxy resins and composites IV. Advances in polymer science, vol. 80. Berlin, Heidelberg: Springer; 1986. p. 101–23. https://doi.org/10.1007/3-540-16423-5_13.

[18] Mohan J, Ivanković A, Murphy N. Effect of prepreg storage humidity on the mixed-mode fracture toughness of a co-cured composite joint. Compos Part A Appl Sci Manuf 2013;45:23–34. https://doi.org/10.1016/J.COMPOSITESA.2012.09.010.

[19] Ledru Y. Etude de la porosité dans les matériaux composites stratifiés aéronautiques. PhD thesis. Institut National Polytechnique de Toulouse; 2009.

[20] de Parscau du Plessix B, le Corre S, Jacquemin F, Lefebure P, Sobotka V. Improved simplified approach for the prediction of porosity growth during the curing of composites parts. Compos Part A Appl Sci Manuf 2016;90:549–58. https://doi.org/10.1016/J.COMPOSITESA.2016.08.024.

[21] Kermani NN, Simacek P, Advani SG. Porosity predictions during co-cure of honeycomb core prepreg sandwich structures. Compos Part A Appl Sci Manuf 2020;132:105824. https://doi.org/10.1016/J.COMPOSITESA.2020.105824.

[22] Kamal MR. Thermoset characterization for moldability analysis. Polym Eng Sci 1974;14:231–9. https://doi.org/10.1002/PEN.760140312.

[23] Karkanas PI, Partridge IK, Attwood D. Modelling the cure of a commercial epoxy resin for applications in resin transfer moulding. Polym Int 1996;41:183–91. https://doi.org/10.1002/(SICI)1097-0126(199610)41:2.

[24] Kenny JM, Maffezzoli A, Nicolais L. A model for the thermal and chemorheological behavior of thermoset processing: (II) Unsaturated polyester based composites. Compos Sci Technol 1990;38:339–58. https://doi.org/10.1016/0266-3538(90)90020-6.

[25] Trivisano A, Maffezzoli A, Kenny JM, Nicolais L. Mathematical modeling of the pultrusion of epoxy based composites. Adv Polym Technol 1990;10:251–64. https://doi.org/10.1002/ADV.1990.060100402.

[26] Sharp N, Li C, Strachan A, Adams D, Pipes RB. Effects of water on epoxy cure kinetics and glass transition temperature utilizing molecular dynamics simulations. J Polym Sci B Polym Phys 2017;55:1150–9. https://doi.org/10.1002/POLB.24357.

[27] Lionetto F, Moscatello A, Maffezzoli A. Effect of binder powders added to carbon fiber reinforcements on the chemoreology of an epoxy resin for composites. Compos B Eng 2017;112:243–50. https://doi.org/10.1016/J.COMPOSITESB.2016.12.031.

[28] Kenny JM, Opalicki M. Influence of the chemorheology of toughened epoxy matrices on the processing behavior of high performance composites. Makromol Chem Macromol Symp 1993;68:41–56. https://doi.org/10.1002/MASY.19930680106.

[29] Lionetto F, Buccoliero G, Pappadà S, Maffezzoli A. Resin pressure evolution during autoclave curing of epoxy matrix composites. Polym Eng Sci 2017;57:631–7. https://doi.org/10.1002/PEN.24568.

[30] Buccoliero G, Lionetto F, Pappadà S, Maffezzoli A. The effect of diffusion and pressure on porosity in composites. In: ECCM18 - 18th European conference on composite materials, athens, Greece; 2018.

[31] Darcy H. Les fontaines publiques de la ville de Dijon: exposition et application des principes à suivre et des formules à employer dans les questions de distribution d'eau: ouvrage terminé par un appendice relatif aux fournitures d'eau de plusieurs villes, au filtrage des eaux et à la fabrication des tuyaux de fonte, de plomb, de tôle et de bitume, vol. 2. Paris, France: Librairie des corps impériaux des ponts et chaussées et des mines; 1856.

[32] Dei Sommi A, Lionetto F, Maffezzoli A. An overview of the measurement of permeability of composite reinforcements. Polymers 2023;15:728. https://doi.org/10.3390/POLYM15030728.

[33] Fick AV. On liquid diffusion. The London, Edinburgh, and dublin philosophical magazine and. J Sci 1855;10:30–9. https://doi.org/10.1080/14786445508641925.

[34] Korkees F, Swart R, Barsoum I. Diffusion mechanism and properties of chemical liquids and their mixtures in 977-2 epoxy resin. Polym Eng Sci 2022;62:1582–92. https://doi.org/10.1002/PEN.25946.

[35] Brand RA, Brown GG, McKague EL. Processing science of epoxy resin composites. 1984. San Diego, CA.

[36] Bharadwaj RK. Modeling the barrier properties of polymer-layered silicate nanocomposites. Macromolecules 2001;34:9189–92. https://doi.org/10.1021/MA010780B/ASSET/IMAGES/LARGE/MA010780BF00003.JPEG.

[37] Antonucci V, Giordano M, Inserra Imparato S, Nicolais L. Autoclave manufacturing of thick composites. Polym Compos 2002;23:902–10. https://doi.org/10.1002/PC.10487.

[38] Maffezzoli A, Grieco A. Optimization of parts placement in autoclave processing of composites. Appl Compos Mater 2013;20:233–48. https://doi.org/10.1007/S10443-012-9265-8/FIGURES/8.

[39] Antonucci V, Giordano M, Inserra Imparato S, Nicolais L. Analysis of heat transfer in autoclave technology. Polym Compos 2001;22:613–20. https://doi.org/10.1002/PC.10564.

[40] Online materials information resource - MatWeb n.d. https://www.matweb.com/. [Accessed 23 February 2023].

[41] Lionetto F, Montagna F, Maffezzoli A. Out-of-plane permeability evaluation of carbon fiber preforms by ultrasonic wave propagation. Materials 2020;13:2684. https://doi.org/10.3390/ma13122684.

[42] Standard test method for moisture absorption properties and equilibrium conditioning of polymer matrix composite materials n.d. https://www.astm.org/d5229_d5229m-20.html. [Accessed 23 February 2023].

[43] Standard test methods for density and specific gravity (relative density) of plastics by displacement n.d. https://www.astm.org/standards/d792. [Accessed 23 February 2023].

[44] Dilonardo E, Nacucchi M, de Pascalis F, Zarrelli M, Giannini C. High resolution X-ray computed tomography: a versatile non-destructive tool to characterize CFRP-based aircraft composite elements. Compos Sci Technol 2020;192. https://doi.org/10.1016/J.COMPSCITECH.2020.108093.

[45] Buck AL. New equations for computing vapor pressure and enhancement factor. J Appl Meteorol Climatol 1981;20:1527–32. https://doi.org/10.1175/1520-0450(1981)020<1527:NEFCVP>2.0.CO;2.